IMPACT OF QUANTUM CONFINEMENT ON THE FUNCTIONAL PROPERTIES OF ULTRA-THIN FILMS

Lorenzo Matteo Ferri

Department of Physics 'A. Pontremoli', University of Milan, via Celoria 16, 20133 Milan, Italy

Abstract: This paper examined the impact of managers' ingratiation on workers' affective commitment in tourism related business organizations in Port Harcourt. The paper adopted a cross-sectional survey research design, involving a population of 170 workers. The research data were collected through questionnaire and analyzed using Spearman's Rank Order Correlation Coefficient (rs). It was found that managers' ingratiation has become a referent power factor which managers in the tourism sector have used to elicit and sustain workers affective commitment. The paper concludes that managers' flattery behavior to appear likeable is a strong affective commitment factor in the workplace. Based on this, the paper recommends that managers should build on their referent power to enhance their charismatic capital necessary to engender workers' emotional and selfless interest, dedication to job, sense of belongingness and civic virtue.

Keywords: manager's ingratiation, affective commitment, downward impression management, upward impression management and organizational commitment.

Introduction

The physical properties of thin films are vital for many technological applications, ranging from optical mirrors to solar cells [1, 2], and they are also of interest for fundamental condensed matter physics. For example, our everyday life would be unthinkable without the achievements of microelectronics, a revolution that began with the discovery of transistors [3]. Ever since, the main strategy to make more powerful electronic devices is to shrink the size of semiconductor blocks in a microchip, with the newest types of MOSFET reaching sizes in the range between 7 nm and 22 nm. A different strategy to push the boundaries of computing power is provided by quantum computers. These are based on qubits, which are physically realized by ultra-thin superconducting elements in the thickness range from few tens of nanometers to about 100 nm. Thin films of superconducting materials are also promising as an alternative route to microelectronics, thanks to the recently discovered supercurrent field effect, where electric fields (EFs) are used to suppress the supercurrent in ultra-thin films [4, 5]. Metallic and superconducting ultra-thin films are also of great technological importance for their thermal properties, in particular for their application as single-photon detectors and, again, as components for superconducting nanoelectronics. In all these applications, it is crucial to effectively control the heat removal and the heat dissipation at cryogenic temperatures, which ultimately means tackling phonon transport problems under nanoscale confinement.

At the very heart of the problem of understanding superconductivity, or electronic and heat transport, in nanometric thin films, lies the fundamental problem of effectively describing the propagation of wavefunctions in nano-confinement. The most difficult problem is posed by the presence of an interface which impedes or limits the propagation of the wavefunction across it. This is because of the irregularity of the interface, which is unavoidable in any experimentally realized film. Even for the most regular surface of a perfectly crystalline film with no defects, assuming that the wavefunction vanishes exactly at the same coordinate of the surface is a strong idealization, made unphysical by the atomic roughness of the surface.

A new approach, originated from the study of elasticity of thin liquid films [6], has recently been investigated, which can manage the description of wavefunctions under nano-confinement without having to assume a fixed hard-wall boundary condition (BC).

Furthermore, this theory provides a simple way of obtaining analytical closed-form expressions for key physical quantities, such as the electronic density of states (DOSs), the phonon DOS, the Fermi energy, as a function of the film thickness. This allows the theory to be incorporated into microscopic frameworks and models of electronic and vibrational properties. Agreement with experimentally observed quantities has been achieved over the past few years for different quantities (electrical conductivity, superconducting critical temperature, specific heat) and for diverse materials, ranging from semiconductors to metals to insulators. Particularly striking has been the prediction of the superconducting critical temperature as a function of nanometric film thickness for two real materials, aluminum and lead, with no adjustable parameters, by implementing this quantum confinement strategy within the Eliashberg theory of superconductivity [7].

In this Perspective paper we attempt to provide a succinct pedagogical introduction to these latest developments. We will consistently focus on thin films that remain 3D even in the quasi-2D or ultra-thin (sub-nanometer) limit. This treatment leaves the perfect 2D limit, i.e. the atomic monolayer, out of the current discussion. This choice is motivated by the fact that the basic physical laws change discontinuously upon going from a 3D multi-layer to a perfectly 2D monolayer, as reflect e.g. in different functional forms of the DOSs for both phonons and electrons and in many other properties and phenomena, the mechanism of which radically changes upon taking the perfect monolayer limit. For a discussion of these issues, cf [8].

1. Quantum confinement of wavefunctions in real materials

We schematize the thin film as a 3D material with confinement along the vertical z direction, and consider it unconfined along the two other Cartesian directions, i.e. in the xy plane, as schematically depicted in figure 1 for the generic case of non-interacting quasiparticles (e.g. phonons or electrons). For electrons, the red sphere is the Fermi sphere, while for phonons it is the Debye sphere.

As derived in [8–11], along the direction θ (cfr figure 1(a)), plane-wave quasiparticles with wavelength

$$\lambda > \lambda_{\max} = \frac{L}{\overline{\cos\theta}} \qquad (1)$$

cannot propagate in the thin film. Here, the polar angle θ of the propagation direction is measured with respect to the vertical z axis (cfr figure 1(a)).

As stated in all quantum mechanics textbooks, the momenta k_x, k_y, k_z of a quantum particle in a (small) box are, in general, discretized whenever standard vanishing (or hard-wall) BCs are chosen for the governing Schrödinger equation. In particular, by imposing that the quasiparticle wavefunction ψ vanishes exactly at the borders of the, e.g. rectangular, box, one obtains plane-wave forms of the type $\psi \sim \sin(k_x x)\sin(k_y y)\sin(k_z z)$. The hard-wall BCs lead to a discrete set of values, $k_z = \pi n/L$, with n an integer number. Accordingly, one expects the minimum wavevector in the system to be given by:

$$k_{z,min} = \pi/L. \qquad (2)$$

However, the assumption that the minimum value of k_z is equal to π/L is valid only when the standard hard-wall BCs are strictly enforced at the boundaries of the rectangular box.

This is not what one observes in a 'real' nanoconfined system, where the minimum value of k_z can be much smaller than π/L. To exemplify this point with data, we report below, in figure 2, recently published results from atomistic MD simulations for amorphous ice thin films (figure 2(a) shows a rendering of the simulated system). The data show clearly that k_z can be much smaller than π/L: indeed, it can be even $\pi/2L$, i.e. a factor of 2 smaller.

The ultimate reason for this observation, lies in the unavoidable atomic-scale roughness and irregularities of the interface of the thin film, an effect which becomes ever more important for ultra-thin films just a few nanometers thick or thinner.

Even for a perfectly crystalline thin film with no defects in the inner atomic layers, the interface presents atomic roughness or, even, significant structural disorder as demonstrated in [12]. This is illustrated on the example of the interface of crystalline copper, in figure 3(a).

With reference to figure 3(b), in a real-life thin film with atomic roughness of the interface, the position at which the wavefunction vanishes along the confinement z axis, will be a function of the in-plane coordinates, x and y. This is a genuine disorder effect, whereby k_z is no longer a good quantum number, since values of k_z will be $n\pi/L(x,y)$ where L is not fixed once and for all, but varies randomly with x and y. Indeed, it is well known from quantum mechanics, that momentum is a good quantum number for hard-wall or periodic BCs
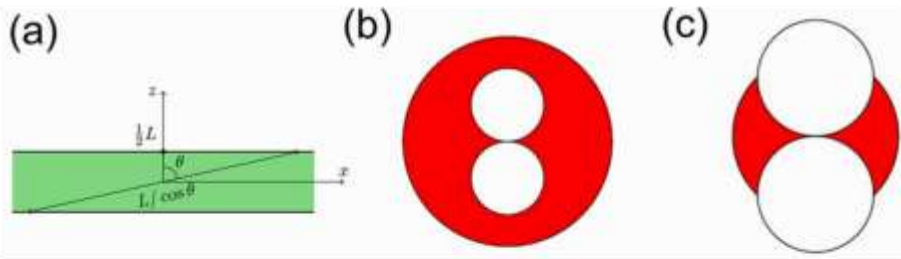
Figure 1. Panel (a) shows the thin film geometry in real space (confined along the z-axis but unconfined along the x and y axis), with the maximum wavelength of a free carrier that corresponds to a certain polar angle θ. Panels (b) and (c) shows the corresponding geometry of occupied quasiparticle states in k-space. For free electrons, the outer Fermi sphere (of radius k_F) contains two symmetric spheres of hole pockets (states suppressed by confinement), i.e. states in k-space that remain unoccupied due to confinement along the z-axis. In (b), for weak confinement, the two hole pockets are well within the Fermi surface, which remains spherical. In (c), for strong confinement (e.g. quasi-2D films), the hole pockets of forbidden states have grown to the point that the Fermi surface gets significantly distorted into a surface belonging to a different homotopy group $\mathbb{Z}$. See [8–10] for a detailed mathematical derivation of these results.
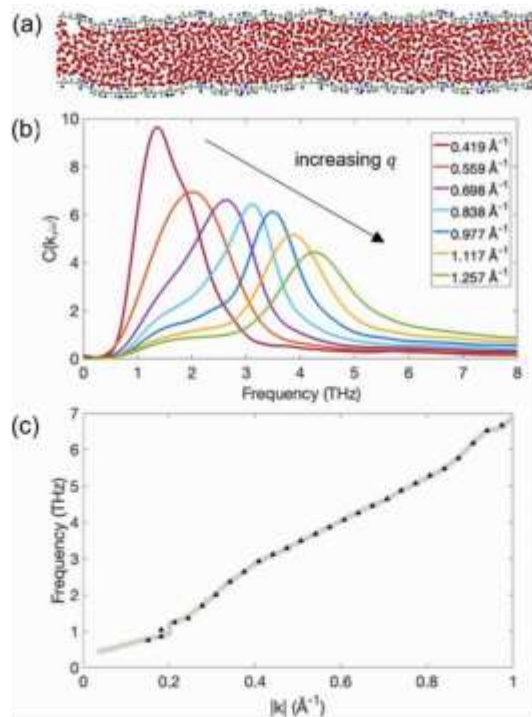
Figure 2. (a) Rendering of an amorphous ice ultra-thin film sandwiched between graphene oxide membranes, from atomistic simulations. (b) The longitudinal current correlations spectrum at different k with fixed $k_z = 0.07\text{Å}^{-1}$. The arrow indicates the motion of the intensity peak upon moving the wave-vector k. (c): The dispersion relation as a function of $|k|$. The grey line represents the computed dispersion relation with wavevector parallel to the xy plane. The black triangles represent the dispersion relation with wavevector $k_z = 0.07\text{Å}^{-1}$. Adapted from [11]. CC BY 4.0.

only, but not for open BCs. As a result, in a real-life thin film there is no discretization of k_z anymore, unlike in an idealized, perfect and smooth rectangular box. It should also be noted that, for a significantly irregular surface, the two white spheres of hole pockets would also have a corresponding 'roughness'. However, by taking the average over the roughness, one would retrieve the two perfect white spheres of figure 3(b). Hence, the theory evaluated using the two perfect white spheres is correct

in an average sense, modulo possible local small fluctuations of the hole pockets envelope around the mean given by the two perfect spheres.

Another consequence of this important fact is the following: if the sample is extended in the xy plane, as it is for thin films, k can still be treated as a quasi-continuous variable [9, 13], because $|\mathbf{k}| = k = 2\pi/\lambda$ obeys the following relation [14, 15]:

$$\frac{1}{\bar{k}^2}\left(k_x^2 - k_y^2 + k_z^2\right) = 1 \tag{3}$$

The confinement-induced cutoff on λ, equation (1), remains valid, in good approximation, also when
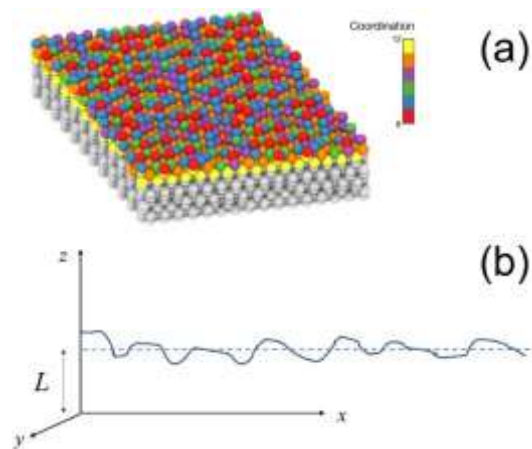
Figure 3. (a) Rendering of a perfectly crystalline copper thin film prepared at 500 K, with evidence of strong disorder in the uppermost atomic layer (interface) [12]. Different colors of atoms in the interface layer correspond to different local crystallographic structures and coordination numbers (different colors correspond to different coordination numbers as explained by the legend). Image courtesy of Massimo Delle Piane. (b) Schematic of an irregular interface of a thin film of thickness L along the confinement dimension (vertical z axis, consistent with figure 1(a)). The irregularity of the interface is greatly exaggerated for illustrative purposes.

the irregularities of the interface are such that k_z is not discretized. The cutoff condition means that a number of quasiparticle states in k-space are suppressed due to the confinement along the z direction of the film.

We shall see what the implications of this cutoff are for the distribution of momentum states of electrons and phonons in the following sections.

2.   Phonons

Let us reformulate the condition for the cutoff, equation (1), in terms of the wavevector:

$k_{min} = 2\pi \cos\theta/L. \tag{4}$

This is a parametric equation for two identical, mirror-image spheres, across the $k_x - k_y$ plane in a 3 D k-space [10], and is schematically depicted in figures 1(b) and (c). These two (white) spheres, which are contained within the Debye sphere (red), correspond the unoccupied states that cannot be populated due to the confinement. As the confinement is further enhanced (or L is decreased), these two white spheres of unoccupied states eventually make contact with the Debye sphere's surface. With additional confinement, the surface corresponding to the highest momentum becomes non-spherical, as shown in figure 1(c).

3.1. Vibrational DOSs (VDOSs) of thin films

The occupied volume in k-space can be evaluated exactly using basic solid geometry, as shown in [8, 9], and reads as:

$$\text{Vol}_k = \frac{Lk^4}{2}. \qquad (5)$$

The number of states in k-space with $k < k'$ then readily follows as:

$$N(k < k') = \frac{V}{(2\pi)^3} \frac{Lk^4}{2}, \qquad (6)$$

where V is the total volume of the sample. The phonon DOSs in the thin film then follows immediately, upon defining the speed of sound v such that $\omega = vk$, as:

$$g(\omega) = \frac{d}{d\omega} N(\omega < \omega') = \frac{V}{4\pi^3 L} \frac{\omega^3}{v^4} \qquad (7)$$

which exhibits a cubic frequency dependence $\sim \omega^3$ that was verified both experimentally (inelastic neutron scattering) and by molecular dynamics simulations in [11]. Importantly, the ω^3 law holds for both crystalline thin films as well as for completely amorphous thin films. The above VDOSs is for just one phonon polarization, and a factor of three has to be implemented when computing the total internal
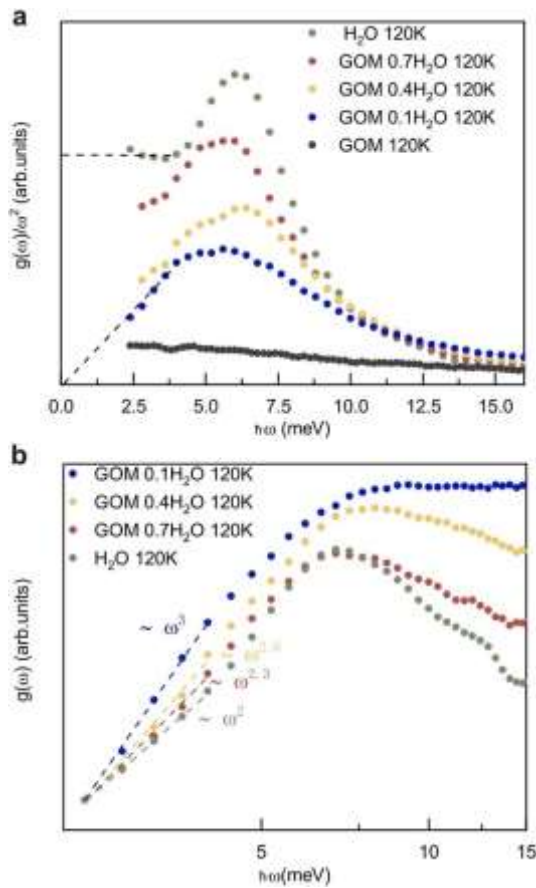
Figure4. (a) Debye-normalized VDOS of ice thin films (sandwiched between graphene oxide layers) as measured by inelastic neutron scattering. Different curves refer to varying thickness L in the range 0.7–2 nm, with L decreasing from top to bottom (the bottom curve is the dry graphene oxide background signal). The top curve exhibits the quadratic Debye law expected for bulk solids, whereas the blue curve exhibits the ω^3 law derived for nanometric thin films. (b) Phonon density of states (not normalized) for a thin film of crystalline ice, of thickness L in the range 0.7–2 nm, with L decreasing from bottom to top. Adapted from [11]. CC BY4.0.

energy U [14]. This law is to be contrasted with the standard Debye law for the phonon DOSs, exhibiting, instead, a quadratic frequency-dependence:

$$g(\omega) = \frac{V\,\omega^2}{2\pi^2\,v^3}. \qquad (8)$$

We also note the linear dependence on the film thickness, L. The above ω^3 law for the phonon DOSs of thin films has been experimentally verified by inelastic neutron scattering for ultra-thin films of ice of thickness $L \approx 1$ nm, as shown in figure 4.

3.2. Specific heat of thin films

Since the internal energy of the system can be written as an integral over the VDOS, upon taking the first derivative of the internal energy with respect to the temperature T, one readily obtains the following formula for the heat capacity of thin films:

$$C_v = 120\,\zeta\,(5)\,\frac{3}{4\pi^3}\,\frac{L}{v^4}\,k_B\left(\frac{k_B T}{h}\right)^4. \qquad (9)$$

This formula exhibits a new $\sim T^4$ dependence of the heat capacity on temperature, and a new dependence $\sim L$ on the film thickness. The $\sim T^4$ dependence of the specific heat of thin films is radically
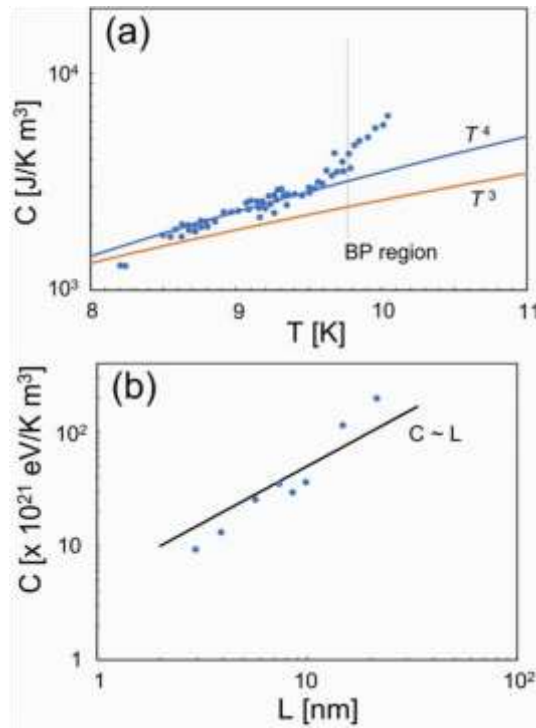
Figure5. (a) Comparison between the T^4 temperature dependence of the phonon heat capacity predicted by equation (9) (blue line) and experimental data (circles) on NbTiN thin films ($L = 6$ nm), Adapted figure with permission from [16], Copyright (2024) by the American Physical Society. There is only one parameter in the comparison, which is the speed of sound $v \sim 4000$ ms^{-1}, here taken as a characteristic value of speed of sound in metals and a plausible value for this material. The Debye T^3 scaling (orange line) is also shown for reference, along with a dashed demarcation line for the onset of the boson peak phenomenon in this class of materials [17]. (b) Comparison between the predicted linear scaling of specific heat with thickness L and experimental data for NbTiN thin films.

different from the textbook Debye law $\sim T^3$, and is a genuine quantum confinement effect resulting from the cutoff argument equation (1).

A preliminary comparison of the heat capacity predicted by equation (9) with experimental data on NbTiN thin films can be seen in figure 5.

These results pave the way for a new understanding of other thermal properties of thin films, including the thermal conductivity. Indeed, the thermal conductivity can be expressed in terms of an integral over the specific heat [18], or equivalently, over the VDOS [19, 20]. In particular, the mechanistic understanding of quantum confinement effects on the phonon statistics, i.e. on the VDOS and on the specific heat, outlined above may represent a solid basis to arrive at a similar mechanistic understanding of the ubiquitously observed increase of thermal conductivity with film thickness [20–22]. This also includes the important case of graphene [23–25], which, in its monolayer state, exhibits an extremely high thermal conductivity [26].

3. Electrons

We now consider a metallic thin film, and work in the free-electron approximation. Also in this case, due to the unavoidable roughness of the film surface, the electron wavefunction will not vanish exactly on the surface of an idealized perfectly rectangular box. Hence, due to this and due to the lack of confinement in the xy plane, also in this case, k_z is no longer a good quantum number and we do not expect it to be quantized.

4.1. Fermi surface topology of thin films

The Fermi sphere of a thin film is schematically depicted in figures 1(b) and (c). There are two hole-pocket spheres (symmetric with respect to the origin, along the k_z axis), which represent the unpopulated states in k-space due to confinement. This is because equation (1) applies also in this case. For a thin film of thickness L, this reduction of the available volume for free carriers in momentum (k) space is evaluated exactly as (cfr figure 1(b)):

$$\text{Vol}_k = \frac{4}{3}\pi k^3 - 2\frac{4}{3}\pi \left(\frac{\pi}{L}\right)^1. \qquad (10)$$

Upon reducing the film thickness further below a threshold $L_c = (2\pi/n)^{1/3}$, where n is the free carrier concentration, one encounters a topological-type transition first described in depth in [9]. At this transition, the Fermi surface undergoes a distortion from the trivial homotopy group $\pi_1(S^2) = 0$ of the spherical surface to a surface belonging to a different homotopy group Z, with the new topology depicted in figure 1(c). In this
situation, the available volume in k space becomes (again see [9] for a full derivation):

$$\text{Vol}_k = -V_{\text{inter}} - \frac{4\pi k^3}{3} - \frac{Lk^4}{2}, \qquad (11)$$

where V_{inter} denotes the intersection of the two white spheres of hole pockets (states suppressed by confinement) with the original Fermi sphere (figure 2). It could be interesting, in future work, to investigate whether the above topology of the Fermi sea does include two different Fermi surfaces, for holes and electrons, in which case the Bianconi–Perali–Valletta theory [27, 28] would predict a Fano–Feshbach resonance between two superconducting gaps that could be experimentally checked upon.

4.2. Electron DOSs at varying film thickness

From this, the electronic DOSs $g(\epsilon)$ of free carriers can be easily evaluated [9]:

$$g(\epsilon) = \begin{cases} \frac{VLm^2}{2\pi^3\hbar^4}\epsilon, & \text{if } \epsilon < \frac{2\pi^2\hbar^2}{mL^2} \\ \frac{V(2m)^{3/2}}{2\pi^2\hbar^3}\epsilon^{1/2}, & \text{if } \epsilon > \frac{2\pi^2\hbar^2}{mL^2} \end{cases} \qquad (12)$$

.

with a crossover from the linear-in-energy regime at low energies to the standard Fermi-gas square-root at higher energies.
The crossover is located at an energy $\epsilon^* = \frac{2\pi^2\hbar^2}{mL^2}$, which depends on the film thickness L.

4.3. Fermi energy as a function of film thickness

We are now able to derive the Fermi energy ϵ_F for this system. Since the total number of electrons N in the sample is conserved, we have (always at $T = 0$):

$$N = \int_0^{\epsilon_F} g_s g(\epsilon)\,d\epsilon, \qquad (13)$$

with the spin-degeneracy factor $g_s = 2$. Upon plugging-in the electron DOSs of the thin film given by equation (12), and evaluating the integral in a piecewise fashion, we obtain

$$N = \frac{4 V(2m)^{3/2}}{3(2\pi)^3\hbar^3}\epsilon_F^{3/2} - \frac{4\pi V}{2}\frac{3L}{3}, \qquad (14)$$

and, therefore,

$$\epsilon_F = \epsilon_{\text{bulk}F}\left(1 + \frac{2}{3}\frac{\pi}{nL^3}\right)^{2/3}, \qquad (15)$$

where $n = N/V$ is the free-carrier density in the sample. One can notice the explicit dependence of the Fermi energy on the film thickness L. The above dependence of Fermi energy on the film thickness recovers expressions that were already proposed in the literature based on the assumption of perfectly smooth rectangular boxes with vanishing hard-wall BCs [29, 30].

Under conditions of strong confinement, it may as well happen that $\epsilon_F < \epsilon^*$. The value of film thickness L_c where this happens depends solely on the free-carrier density n and is given by:

$$L_c = \left(\frac{2\pi}{n}\right)^{1/3}. \quad (16)$$

In this regime, we have only one integral since the linear DOS extends up to ϵ_F. A simple evaluation gives:

$$\epsilon_F = \frac{\hbar^2}{m} \left[\frac{(2\pi)^3 n}{L}\right]^{1/2}. \quad (17)$$

Upon collecting results for the two regimes, as usual, we can write the Fermi energy as a function of the film thickness across the entire regime of free-carrier density as a piecewise function:

$$\epsilon_F = \begin{cases} \epsilon_F^{bulk}\left(1 + \frac{2}{3}\frac{\pi}{nL^3}\right)^{2/3} & \text{if } L > L_c = \left(\frac{2\pi}{n}\right)^{1/3} \\ \frac{\hbar^2}{m}\left[\frac{(2\pi)^3 n}{L}\right]^{1/2} & \text{if } L < L_c = \left(\frac{2\pi}{n}\right)^{1/3}. \end{cases} \quad (18)$$

4.4. Resistivity of ultra-thin semiconductor films

The resistivity of thin films has been a topic of intense research since the advent of modern quantum mechanics and statistical physics, due to its immense technological significance. Most of the attention has been traditionally focused on the role of the surface, and, in particular, on the enhanced scattering of free carriers by the interface (in addition to standard scattering by defects and phonons as in the bulk material). In simple terms, thinner films have comparatively more specific interface, such that surface-scattering events will become increasingly more important contributions to the resistivity. As a result, the resistivity increases upon decreasing the film thickness, which is, indeed, what one observes experimentally. This mechanism lies at the heart of the most widely used theoretical framework for the resistivity and conductivity of thin films, known as the Fuchs−Sondheimer (FS) theory. Originally developed by Fuchs in 1938 [31] and later refined by Sondheimer [32], the theory is based on an approximate solution to the Boltzmann kinetic equation for the population balance of free carriers, by taking the above mentioned surface-scattering processes into account. As reported by Sondheimer [32], simple closed-form expressions for the resistivity contribution of surface scattering are obtained for thick films and thin films, respectively, as $\rho_s/\rho_0 = [1+3/(8\kappa)]^{-1}$ and $\rho_s/\rho_0 = \{4/[3\kappa \ln(1/\kappa)]\}^{-1}$, with $\kappa = L/\ell$ where ℓ is the mean free path in the bulk material [32]. E.g. for silicon, $\ell \approx 20$ nm, hence the crossover between the two formulae occurs around 10 nm.

The most recent *ab-initio* calculations have been compared with the predictions of the FS theory in [33]. For the case of Cu thin films over a very broad thickness range (spanning from hundreds of nm to about 5 nm), the agreement is not always optimal, in particular for ultra-thin films below 10 nm of thickness [33]. While phenomenological approaches based on the full-band model provide a much better fitting of the *ab-initio* data, still the quantum confinement effects have not been taken into account.

In the following, based on reference [34], we propose a combined FS-quantum confinement model which is able to describe the thickness-dependent resistivity of ultra-thin silicon films in a regime where the available experimental data cannot be described by the FS theory alone or by other approaches.

4.5. Resistivity of c-Si ultra-thin film

The Fermi level μ is defined as the Fermi energy ϵ_F at zero temperature. By thus setting $\epsilon_F \equiv \mu$, for consistency with the semiconductor physics literature, this quantity is given by:

$$\mu = \begin{cases} \mu_\infty \left(1 + \frac{2}{3}\frac{\pi}{nL^3}\right)^{2/3} & \text{if } L > L_c = \left(\frac{2\pi}{n}\right)^{1/3} \\ \frac{(2\pi)^{3/2}\hbar^2}{m}\left(\frac{n}{L}\right)^{1/2} & \text{if } L < L_c = \left(\frac{2\pi}{n}\right)^{1/3} \end{cases} \quad (19)$$

where μ_∞ is the Fermi level of the bulk material.

We consider c-Si semiconductor thin films, which are either intrinsic or weakly-doped such as e.g. the *ex situ*-doped thin films studied recently in [35]. Since, in these materials, there are well-known issues of dopant deactivation, we are going to use the equations for the free-carriers concentration as for intrinsic semiconductors.

For these systems, the concentration of free carriers varies in a broad range, from a lower bound that coincides with the intrinsic material, $n \sim 10^{16}\,\text{m}^{-3}$, to an upper bound of $n \sim 10^{25}\,\text{m}^{-3}$, as noted in [35]. Here we focus our theoretical analysis on a regime of very weak n-doping where $n \sim 10^{16} - 10^{20}\text{m}^{-3}$.

In these conditions, L_c is of the order of hundreds of nanometers, and we can thus safely operate in the regime $L < L_c$, using the second of the two relations reported in equation (19). In this regime, the concentration of free carriers is given as [14]:

$$\overline{n_i = \sqrt{n_c(T)n_v(T)}\exp(-E_g/2k_BT)} \quad (20)$$

where $n_{c(T)} = 2\left(\frac{m_e^* k_B T}{2\pi\hbar^2}\right)^{3/2}$ and $n_{v(T)} = 2\left(\frac{m_h^* k_B T}{2\pi\hbar^2}\right)^{3/2}$. Here, m^*_e and m^*_h are the effective masses of electrons and holes, respectively, and E_g is the gap energy. The latter is related to the Fermi level via:

$$\mu = \frac{1}{2}E_g + \frac{3}{4}k_BT\ln(m_h^*/m_e^*). \quad (21)$$

Since the holes are lighter than the electrons, iwe can write:

$$E_g = 2\mu - \text{const}\cdot k_BT \quad (22)$$

where const > 0. This relation reflects the fact that the Fermi level falls exactly in the middle of the energy gap at $T = 0$, while it is shifted upwards towards the bottom of the conduction band at room temperature. Because, in the thin film, the Fermi level μ is a function of the thickness L via equation (19), the above relation implies that the energy gap E_g is a function of L. In particular, because the Fermi level increases upon decreasing L, the gap energy E_g must increase upon decreasing L (this may no longer be true for monolayer semiconductors where the band structure topology can change significantly, which may lead to a smaller energy gap as demonstrated for PbS monolayers in [36]). Working in the weakly n-doped regime, the conductivity σ is given by:

$$\sigma = (n_i + n_d)e\mu_e \quad (23)$$

where n_d represents the concentration of free carriers due to n-doping, e.g.

$n_d \approx [n_c(T)N_d]^{1/2}\exp(-E_d/2k_BT)$, where N_d is the concentration of donors and E_d is the ionization energy of the donor impurity atom. In a first approximation which should remain valid for multi-layer thin films, the ionization energy E_d should not differ substantially from its value in the bulk. Hence, one can assume the form of n_d to be independent of the film thickness L, and that the donor atoms' contribution to the L-dependence of the conductivity is negligible. However, this assumption should be treated more carefully upon approaching the $L \to 0$ limit or the perfect monolayer. That is because, in that case, the electron wavefunction becomes significantly squeezed in the z direction compared to the other directions, and also the total electrostatic potential experienced by the ionizing electron could be significantly different from that in the bulk (this is a phenomenon somewhat analogous to the pressure ionization lowering known in plasma physics [37]). Here we shall neglect these effects and leave them for careful consideration in future more microscopically detailed studies.

Furthermore, the mobility $\mu_e = e\tau_e/m_e$ is given in terms of the mean free time between collisions of electrons with phonons and defects, τ_e. Finally, the dependence of the conductivity on the thickness L due to the quantum wave confinement of the electrons is given, in the regime $L < L_c$, by:

$$\sigma = (n_i + n_d)e\mu_e \sim \exp(-const/L^{1/2}). \qquad (24)$$

The corresponding resistivity contribution due to confinement, ρ_c is then

$$\rho_c(L) = 1/\sigma \sim \exp(const/L^{1/2}). \qquad (25)$$

We now combine this effect of quantum confinement on the conductivity, with the surface-scattering as predicted by the FS theory. Assuming that Matthiessen's rule is valid, the different effects of quantum confinement and of surface scattering can be summed up as independent contributions [14] to give the total resistivity $\rho(L)$ as:

$$\rho(L) = \rho_c(L) + \rho_s(L) \qquad (26)$$

where $\rho_s(L)$ is given by the FS theory [32].

Using the form for the confinement-induced resistivity as a function of L given in equation (25) for $\rho_c(L)$ and the asymptotic FS expressions mentioned above for $\rho_s(L)$, one thus obtains the fitting of the experimental data of [35] reported in figure 6.

As is clear from figure 6, down to $L\approx10$ nm, the dominant contribution to the resistivity is given by the FS mechanism from surface scattering (green dashed line). As long as the FS is the dominant contribution, the confinement-induced contribution to resistivity is orders of magnitude smaller. At about $L\approx10$ nm there is a dramatic crossover, with the confinement-induced contribution (orange dashed line in figure 6) taking over with respect to the FS contribution. This now becomes the dominant effect as the thickness is reduced below 10 nm. It is this quantum confinement contribution which is allows the model to capture the sharp increase of resistivity in the range from 10 nm to 4.5 nm. Without this contribution, there is no way that the FS theory could describe the experimental data points. This comparison further corroborates the need of including quantum confinement effects, developed by accounting for the presence of surface roughness even in crystalline thin films, when describing the electronic properties of ultra-thin films. Of course, the caveat always remains that there could be also other, more mundane, contributions to the exponential divergence of resistivity upon shrinking the thickness to the 2D limit. These include absence of percolation or spatial non-uniformity of activated dopants, which are however impossible to distinguish with the current experimental capabilities as one would need extraordinarily detailed data.

4.   Superconductivity of thin films

We can now explore the predictions of the theory for ultra-thin metallic superconductors. We shall assume throughout that the conventional electron–phonon pairing mechanism of electrons is valid. Hence, we will
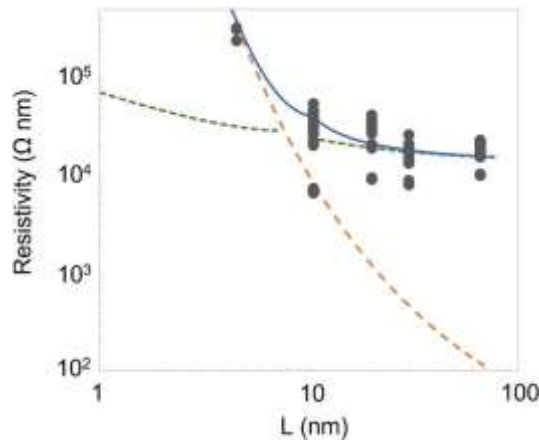
Figure6. Comparison between the theoretical predictions of the proposed model (solid continuous line) obtained by combining the FS surface scattering theory with the electronic confinement model (equation (25)) via Matthiessen's rule, equation (26). The green dashed line represents the FS surface scattering prediction (see text for the corresponding equations) without the electron-confinement correction, whereas the orange dashed line represents the electron confinement correction without the FS contribution, given by equation (25). The symbols (circles) are the experimental data from [35].

first discuss the theory at the level of the Bardeen–Cooper–Schrieffer (BCS) theory [38], for which analytical closed-form expressions of the superconducting critical temperature T_c have been obtained [9].

Subsequently, we shall implement the quantum confinement model into the more general Eliashberg theory of electron–phonon superconductivity, which allows one to describe also higher levels of electron–phonon coupling. Using the Eliashberg theory, it has been recently possible to obtain a quantitative theoretical description of experimental data of T_c as a function of film thickness for aluminum and for lead thin films [7].

5.1. BCS theory for ultra-thin films

Let us start with defining $U_{kk'}$ as the phonon-mediated attractive interaction responsible for the Cooper pairing. In the weak-coupling BCS theory [38], this is simply some negative constant within a Debye-shell beneath the Fermi energy, and zero otherwise:

$$U_{kk'} = \begin{cases} -U, & \text{if } |\epsilon - \epsilon_F| < \epsilon_D \\ 0, & \text{otherwise} \end{cases} \quad (27)$$

Here $\epsilon_D \equiv \hbar\omega_D$ is the Debye energy of the solid, with ω_D the Debye frequency. As usual within BCS theory in its simplest version, the phonons that glue together the Cooper pairs are optical phonons with frequency near ω_D. This fact justifies neglecting the effect of confinement on these phonons (this is because the effects of confinement are mostly affecting acoustic phonons at much lower energy). Using the Bogoliubov method, we obtain [39]

$$\Delta_k = -\sum_l U_{kl}\frac{\Delta_l}{2E_l}\tanh\left(\frac{\beta E_l}{2}\right). \quad (28)$$

This leads to [39]:

$$\frac{1}{U g(\epsilon_F)} = \int_0^{\beta_c\epsilon_D/2} \frac{\tanh(x)}{x}\,dx = \ln(1.13\beta_c\epsilon_D), \quad (29)$$

where β_c indicates the critical value for the Boltzmann factor $\beta = 1/k_B T$, that is, the value at which the transition from normal metal to superconductor occurs. Inverting the relation gives [39]:

$$k_B T_c - 1.13 \epsilon_D \exp\left[\frac{1}{g(\epsilon_F) U} \right]. \quad (30)$$

Clearly, the critical temperature T_c depends strongly (in an exponential fashion) on the electron DOS at the

Fermi level. Upon substituting equation (12) for the electron DOS $g(\epsilon)$ of the thin films and we can evaluate this form of the DOS at the thickness-dependent Fermi energy ϵ_F given by equation (18). We thus obtain:

$$T_c = \begin{cases} \dfrac{4\epsilon_D}{3.52 k_B} \exp\left(-\dfrac{1}{U g^{bulk}(\epsilon_F)\left(1+ \frac{2}{3}\frac{\pi}{nL^3}\right)^{1/3}} \right) & \text{if } L > L_c \\[4ex] \dfrac{4\epsilon_D}{3.52 K_B} \exp\left(-\dfrac{1}{U g^{bulk}(\epsilon_F)} \dfrac{(3\pi^2 n)^{1/3}}{2\pi L n} \right) & \text{if } L < L_c. \end{cases} \quad (31)$$

According to this expression, the T_c is a decreasing function of L for $L > L_c$ and an increasing function of L
for $L < L_c$. Therefore, this expression predicts a maximum in the T_c as a function of thickness L, which occurs exactly at $L = L_c$. This is the thickness value at which the topological-type transition of the Fermi surface occurs, from the Fermi sphere $\pi_1(S^2) = 0$ to the distorted Fermi surface with homotopy group Z, cf figures 1(b) and (c).

The physical origin of this dome of T_c with thickness L lies in the topological distribution of free-electron states in the Fermi sea. For $L > L_c$, cf figure 1(b), as the thickness is reduced, the hole-pocket spheres grow with the consequence that more electron states are pushed to the Fermi surface, which thus increases the electron DOS at the Fermi level, i.e. $g(\epsilon_F)$. In turn, the increase of $g(\epsilon_F)$ within the BCS equation leads to an exponential increase of T_c as L gets reduced. Conversely, if the thickness is lower than L_c, we are now in the situation depicted in figure 1(c). Due to the changed topology of the Fermi surface, as the thickness gets further reduced, in this case, the electron states get more and more spread out over a larger Fermi surface. The consequence of this is that, now, $g(\epsilon_F)$ decreases with further decreasing L. In turn, this leads to a decreasing trend of T_c as the thickness L is further decreased.

5.2. Superconductivity dome as a function of film thickness

The peculiar trend of T_c as a function of film thickness L, with a maximum, has been observed various experimental systems, e.g. in [40] for epitaxial aluminum and also recently in [41] (previous theories also predicted a regime of enhancement of T_c due to confinement [42]). In all these cases, i.e. both in the experimental data-sets as well as in the predictions of the current theory, there is no visible sign of regular oscillations in the trend of T_c vs L, contrary to older theoretical claims [43–46]. The reason for this has to be found, again, in the absence of regular discretization for k_z as explained in section II above.

By using values of the bulk properties, e.g. $g^{bulk}(\epsilon_F)$ and U, close to those reported in the literature, a good agreement between equation (31) and experimental data of Pb ultra-thin films from [47] has been demonstrated in [9], supporting the non-monotonic behaviour with the dome in T_c. However, Pb is a strong-coupling material with a rather high T_c value and large electron–phonon coupling, which should be more rigorously described by the more general Eliashberg theory. This is discussed in what follows.

5.3. Eliashberg theory of superconducting thin films

For the governing equations of the Eliashberg theory of superconductivity in the Migdal approximation we shall refer the reader to the excellent reviews [48, 49]. The standard one-band s-wave Eliashberg equations, when the Migdal theorem holds, can be solved numerically by taking, as the only input, the

64

electron–phonon spectral density $\alpha^2 F(\Omega)$ also known as Eliashberg function (where Ω denotes the phonon frequency). In simple words, this is the phonon frequency-dependent sum over the contributions from scattering processes involving electrons and phonons on the Fermi surface. The Eliashberg function can be either measured experimentally e.g. by tunnelling measurements [50], or computed via *ab-initio* methods [48, 51]. The other key input to the Eliashberg equations is the electron DOS, which the crucial thickness-dependent quantity, and is given by the quantum confinement theory of [9], equation (12) reported above. If one removes the approximations of the infinite bandwidth and of taking the electron DOS equal to a constant (i.e. its value at the Fermi level), the Eliashberg equations are slightly more complex and they become four equations [52]. However, when the electron DOS is symmetrical with respect to the Fermi level, the situation is particularly simple because the non-zero self-energy terms are just two, which facilitates the computation.

This is the scheme used to obtain a quantitative theoretical prediction of the critical temperature T_c as a function of thickness in excellent agreement with experimental data for Al and Pb thin films in [7], shown in here in figure 7.

5.4. Non-superconducting elements may become superconductors near the 2D limit

We learn in high-school that noble metals, such as gold and silver, are excellent conductors of heat and electric current. However, they are not superconductors, or at least their critical superconducting temperature T_c is too low to be measured with standard equipment. We have seen, however, that quantum confinement, in the regime $L > L_c$ can strongly enhance the superconducting T_c of a given material, due to
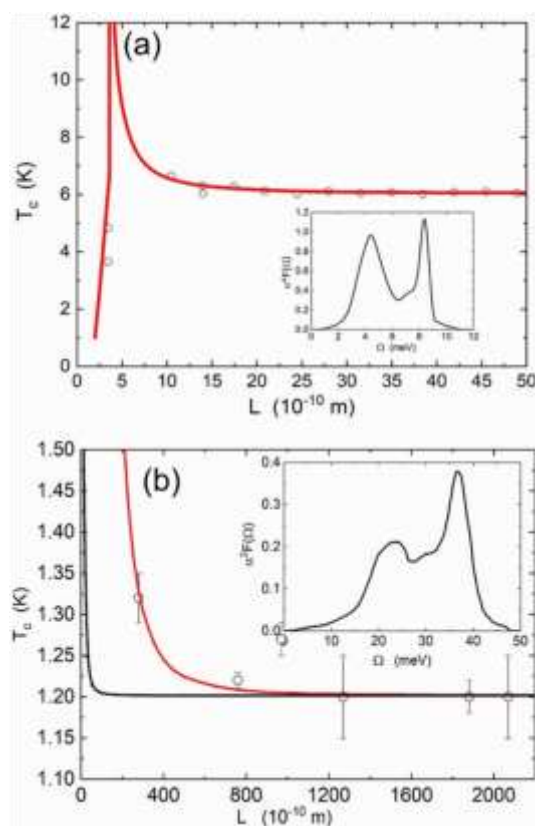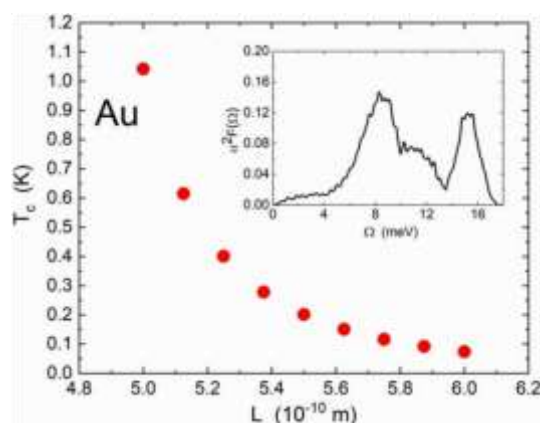
Figure 7. (a) Comparison between Eliashberg theory predictions, accounting for quantum confinement, of the critical temperature T_c as a function of film thickness (solid line) and experimental data for Pb thin films (circles). (b) Comparison between Eliashberg theory predictions, accounting for quantum confinement, of the critical temperature T_c as a function of film thickness (solid line) and experimental data for Al thin films (circles). The experimental data for Pb and Al are taken, respectively, from [47] and [53]. Adapted from [7]. © The Author(s). Published by IOP Publishing Ltd. CC BY 4.0. The insets show the Eliashberg spectral function $\alpha^2 F(\Omega)$ for the two materials.

the growing hole-pockets which push more states to move to the Fermi surface. We have also seen that for good conductors, i.e. for materials with a large concentration of free carriers, n, the maximum at L_c is pushed to extremely low values of thickness, basically to the 2D limit. This implies that one can take advantage of the confinement-induced enhancement of T_c basically down to the 2D limit, for good conductors. This physical consideration is behind the idea of exploring the behaviour of T_c for ultra-thin noble metal films, near the 2D limit. This was done, again by means of Eliashberg theory implementing the quantum confinement model described above and the most accurate *ab-initio* calculations of the Eliashberg function for noble metals. The results, published in [54], are somewhat surprising, as the reveal the possibility that ultra-thin films of gold, about 0.5 nm, may be superconductors with the same critical temperature of aluminum (the latter is the most used material for qubits). The results are shown in figure 8.

Finally, even magnesium (Mg), an alkaline-earth metal that is lighter than aluminum, is well known to be a good conductor but not to be a superconductor. Even in this case, however, quantum confinement leads to such increase in the DOS at the Fermi level, that Mg becomes an excellent superconductor when cast into ultra-thin sub-nanometer sheets. The same type of calculation [55], using Eliashberg theory and the Eliashberg function computed from *ab-initio* simulations, predicts that Mg can achieve a superconducting critical temperature as high as 10 K when the thickness is about 0.4 nm, as shown in figure 9. Also in this case, there are no adjustable parameters in the prediction. If confirmed

experimentally, this would be a particularly attractive discovery for many technological applications (e.g. quantum computing, quantum electronics), because Mg would be a superconductor at temperatures well above the liquid helium boiling temperature.

Objectively, an experimental verification of this prediction is difficult, because the effect may easily be obscured, e.g. by proximity effects. Also, ultra-thin films of gold may be extremely brittle and mechanically unstable. However, good candidate systems to detect this effect have been recently developed experimentally, which include: macroscopically large, nearly freestanding 2D gold monolayers, consisting of nanostructured patches formed on on an Ir(111) substrate and embedding boron (B) atoms at the Au/Ir interface [57]. Another candidate experimental system could be the ultra-thin nanowires obtained via nano-molding [58] , which, in future technical improvements, may reach the atomic-scale thickness.

Figure 8. Eliashberg theory predictions, accounting for quantum confinement, of the critical temperature T_c as a function of film thickness L for gold thin films. The inset shows the Eliashberg spectral function $\alpha^2 F(\Omega)$ as computed via *ab-initio* methods [51]. Adapted figure with permission from [54], Copyright (2024) by the American Physical Society.
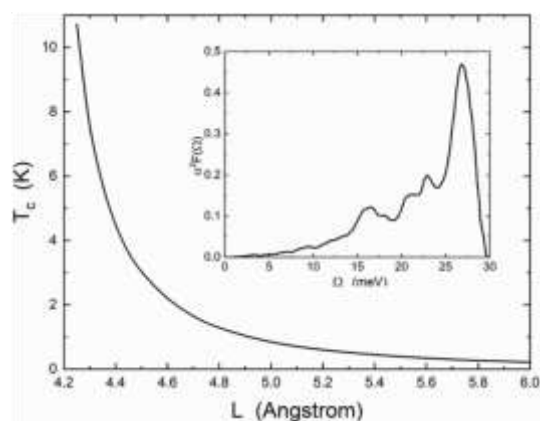
Figure 9. Eliashberg theory predictions, accounting for quantum confinement, of the critical temperature T_c as a function of film thickness L for magnesium (Mg) thin films. The inset shows the Eliashberg spectral function $\alpha^2 F(\Omega)$ as computed via *ab-initio* methods [56]. Reproduced from [55]. CC BY 4.0.

5.5. Tuning the thin film superconductivity with electric fields
Recent experimental work has revealed that superconductivity in thin metallic films can be suppressed by applying a strong enough external DC EF, denoted as E_{cr} [4, 5, 59]. Experimental evidence has shown

that external EFs on the order of ~10^8 Vm^{-1} are required to suppress the supercurrent in metallic thin films with a thickness of around 20 nm [59]. These findings are of great technological importance, because supercurrent field-effect transistors have huge potential for future classical [60, 61] and quantum computation [62] nanodevices.

In spite of this intense experimental activity, the microscopic mechanism by which an external EF is able to penetrate a superconductor on a length-scale much larger than the Thomas–Fermi length of the normal state, has remained unclear. Numerical and experimental evidence has shown that the penetration length of an external static EF into Niobium-based thin films can be as large as 4 nm, hence closer to the London depth than to the Thomas–Fermi length [63, 64]. Some electrodynamic covariant theories [65, 66], building on an original intuition of F. London, seem to justify that an external EF penetrates into the SC phase on a length scale comparable to the London length.

Whatever the exact penetration depth of the EF into the superconductor, standard electrodynamics shows that the EF amplitude decays exponentially from the interface into the thin film, with a characteristic decay length. If the decay length is a few nanometers, the EF will be non-zero also beyond the the decay length, because an exponentially-decaying function is identically zero only at infinite distance. This, in turn, will lead to a finite probability of Cooper pair breakage via tunnelling enabled by the EF. A microscopic theory of this effect, within a simplified version of the Eliashberg theory, has been derived recently in [67]. The theory predicts the critical value of EF needed to suppress superconductivity in metallic thin films, as a function of the film thickness L.

The problem of splitting a Cooper pair by an EF is analogous to the textbook problem of EF-induced dissociation of an s-wave bound state. This is because, within BCS theory, a Cooper pair is described by a s-wave bound state satisfying the Schrödinger equation for two electrons interacting via an effective attractive force [38, 68], with a real-space description originally suggested by Weisskopf [69]. The solution for the bound-state dissociation under an EF is well known [70], and has been used to describe the Cooper pair splitting by an external EF in [67]. The formula for the critical EF magnitude needed to split the Cooper pair is given by [67]:

$$E_{cr} = \frac{2\Delta}{e\xi}, \qquad (32)$$

where Δ is the BCS energy gap, e is the electron charge, and ξ is the coherence length, which is obtained by the solution of Eliashberg equations [48].

Following reference [71], the above formula for E_{cr} can be derived by considering the Schrödinger equation for an electron initially bound in a s-wave bound state (the Cooper pair) of energy depth Δ, and subjected to an external EF of magnitude $E = |-\nabla V|$:

$$\left(\frac{1}{2}\nabla^2 + \mathcal{E} + u(r) - Ez\right)\psi = 0 \qquad (33)$$

where E is the energy, E is the EF magnitude, z is the spatial coordinate along which the EF is pointing, and ψ is the wavefunction. In the above equation, atomic units have been used. Furthermore, the attractive potential is schematically given by a spherical well: $u(r) = -\Delta$ for $0 \leqslant r \leqslant \xi$ and zero otherwise, where Δ is the BCS energy gap and ξ is the coherence length [69]. The solutions to equation (33) are obtained by separation of variables in parabolic coordinates, and can be found in textbooks such as in [70]. From the solution to equation (33), one obtains the characteristic critical field E_{cr} to break the Cooper pair as follows.

While the s-wave bound state (the Cooper pair) is spherically symmetric, the EF is directed along a certain spatial direction, which could be any direction in the solid angle. Hence, as shown with full

details in the textbooks, pp 296–7 of [70], one solves the Schrödinger equation equation (33) in parabolic coordinates, and uses the solution to compute the probability current of the electron escaping away from the bound state in the direction of the EF (i.e. the coordinate z in equation (33)). The result for the probability w of the electron tunnelling away from the bound state, in atomic units, is [70]:

$$w \sim \exp\left(-\frac{2}{3E}\right) \quad (34)$$

where E is the magnitude (absolute value) of the EF. For a s-wave bound state of unitary depth energy and unitary radius, converting from atomic to physical units, the above formula from [70] reads as:

$$w \sim \exp\left(-\frac{2}{3}\frac{E_a}{E}\right) \quad (35)$$

where

$$E_a = 2\frac{R_H}{ea_0}, \quad (36)$$

with R_H the Rydberg energy and a_0 the Bohr radius (both are equal to unity in the atomic units used in Landau's derivation [70]). Hence the critical EF to dissociate the bound state is:

$$E_{cr} = \frac{2R_H}{ea_0}. \quad (37)$$

For a generic s-wave bound state of depth energy Δ and radius ξ, the critical EF needed to dissociate the bound state is thus [67]

$$E_{cr} = \frac{2\Delta}{e\xi}$$

which is just the above formula equation (32).

In the above equation for the critical EF, a possibly material-dependent parameter is the coherence length ξ. The latter is given by [72]:

$$\frac{1}{\xi} = \frac{1}{\xi_0} + \frac{1}{\ell}, \quad (38)$$

where ξ_0 is the intrinsic (Pippard) coherence length, and ℓ is the mean free path. Thin films, such as those used in the supercurrent field effect devices, have a microstructure characterized by microcrystallites, the size of which sets the value of ℓ. Since, typically, $\ell \ll \xi_0$ (because ξ_0 can be tens or hundreds of nanometers), the coherence length ξ is controlled by ℓ, and, hence, by the disorder, and $\xi \approx \ell$. Because for experimental metallic thin film systems the disorder is always present [73], in the form of small grains (crystallites) that are randomly packed, we have $\xi \approx \ell$, and, therefore:

$$E_{cr} = \frac{2\Delta}{e\ell}. \quad (39)$$

Being in the diffusive regime where the coherence length ℓ has a small value is implemented in the Eliashberg spectral function, which is not that of a bulk superconductor but that of a thin film. Knowing the gap energy Δ for a given material from the Eliashberg theory, one can estimate the critical EF E_{cr} for superconductivity suppression inside the film.

For the example of NbN, the values of the critical EF needed to suppress the superconductivity in 10–30 nm-thick thin films are of the order of 10^7 Vm^{-1}, under the assumption of no-screening. This

estimate is one order of magnitude lower than the experimental values of the order of $10^8\,\mathrm{Vm^{-1}}$ reported in the literature for films of comparable thickness [59].

As already mentioned, this estimate still assumes a perfect penetration of the EF inside the sample, or, in other words, does not account for the screening of the EF inside the sample. To compute the magnitude of the external EF that has to be supplied to cause the suppression of superconductivity, the screening effects need to be taken into account. It is easy to show that, with a penetration depth of the EF of about 4 nm [63, 64], the predicted critical value of EF for the suppression of superconductivity becomes of the order of $10^8\,\mathrm{Vm^{-1}}$, in agreement with experimental measurements [59].

5.   Conclusions and outlook

We attempted to provide a holistic view of the effects that quantum confinement has on the physical properties of thin films, with a special attention to the case of ultra-thin films with a thickness lower than 10 nm. The starting point is the basic physics of quantum wave propagation through a slender rectangular box, with confinement along the vertical direction, and no confinement in the orthogonal plane. The confinement imposes a cut-off on the wavelength of the quasiparticles states that can populate the sample, which leads to simple mathematical forms of the corresponding DOSs and k-space topology. Importantly, due to the unavoidable disorder and non-smoothness of the interfacial atomic layers at the surface of the film, there is no discretization of the wavevector k_z along the confinement direction in real-life thin films, because standard hard-wall BCs do not apply (k_z is no longer a good quantum number). This fact cannot be captured by traditional theoretical approaches based on an ideal perfectly smooth rectangular box, but is, instead, well-captured by the new confinement approach reviewed here.

In particular, the thin-film confinement leads to a ω^3 form of the phonon DOS, instead of the ω^2 Debye law, a theoretical prediction that has been confirmed experimentally by inelastic neutron scattering for ultra-thin films of ice [11], with a gradual crossover from ω^3 to ω^2 as the thickness increases, as also confirmed by MD simulations. The ω^3 law for the phonon DOS leads to a T^4 law for the heat capacity of ultra-thin films at low temperature, instead of the Debye T^3 law. In future work, it will be of great interest to use these results for a quantitative theory of thermal conductivity in ultra-thin and quasi-2D materials, such as graphene, van der Waals materials and layered films.

Applying the same analysis of confinement to free electrons in thin metallic films, leads to a simple form of the electron DOS, which features a linear-in-energy trend at low-energy, which then crosses over into the standard square-root behaviour at a characteristic energy that depends on the film thickness and on the free-electron density. The theory also shows how two spherical hole-pockets of forbidden states grow inside the Fermi sphere as the thickness is decreased, up to the point where the spherical Fermi surface transitions into a surface with a different homotopy group Z. This transition coincides with the transition between the two regimes in the electron DOS and with a change of confinement-controlled redistribution of momentum states on the Fermi surface. For thickness $L > L_c$ the growing hole-pockets inside the Fermi sphere push more states towards the Fermi surface, thus increasing the DOS at the Fermi level. Instead, for $L < L_c$, the new Z surface becomes more extended as L keeps decreasing, and therefore the momentum states at the surface become more spread out, implying that the electron DOS at the Fermi level decreases.

This mechanism has fundamental implications for the electronic conduction in ultra-thin films, such as c-Si films with thickness below 10 nm, which fall in the regime $L < L_c$. We have demonstrated that this mechanism of 'dilution' of electron states at the Fermi level of the Z surface leads to an exponential increase of the resistivity upon decreasing the thickness. This effect is superimposed on the FS surface-

scattering contribution and is responsible for the exponential increase of resistivity observed experimentally in [35] , which cannot be explained or reproduced by the FS theory.

The same quantum confinement mechanism is responsible for the dome in the critical temperature for the normal metal-to-superconductor transition as a function of film thickness, observed experimentally in several systems. Again, the maximum in T_c coincides with the critical thickness L_c at which the Fermi surface distortion induced by confinement takes place. Implementation of the the electron DOS as a function of thickness into the BCS theory leads to analytical solutions for the T_c as a function of thickness. For a fully quantitative comparison, implementing the confinement model in the Eliashberg theory of superconductivity has recently led to the first quantitative theoretical description of the T_c as a function of thickness for two experimental systems, i.e. aluminum and lead thin films [7], in excellent quantitative agreement with the available experimental data. The same scheme led to the surprising prediction that few atomic layers of gold can become superconducting with the same T_c of aluminum [54]. Finally, the same confinement model can explain the existence of a critical value of EF to suppress superconductivity in thin films [67], a fact experimentally demonstrated in seminal experiments by Giazotto and co-workers [4].

This holistic framework, which describes electrons, phonons and superconductivity in thin films, can be extended in future work in several directions:

(i)   mechanistic understanding of thickness effect on thermal conductivity of ultra-thin and quasi-2D materials [23] ;

(ii)   extension of the framework to include effects of lattice anharmonicity [74], distortions [75], and structural disorder [76] in the interior of the film (not just the interface);

(iii)   application of the framework to high-temperature cuprates superconductors [77], for which atomically-thin film are now available experimentally [78] ;

(iv)   improve the understanding of dielectric properties of thin films as a function of thickness, from ferroelectric [79] to superconductors [66] ;

(v)   extend the framework to different shapes of 3D nanostructures such as nanowires [80–82], nano-rings [83] (for the latter, see [84]) and Möbius strips [85], quantum-dots supercrystal assemblies [86], 2 D random networks of atomic clusters and nanoparticles [87], and artificial heterostructures of alternating superconductor and normal layers [88].

Data availability statement

No new data were created or analysed in this study.

Acknowledgments

References

Shah A, Torres P, Tscharner R, Wyrsch N and Keppner H 1999 Photovoltaic technology: the case for thin-film solar cells *Science* **285** 692

Ball J M *et al* 2015 Optical properties and limiting photocurrent of thin-film perovskite solar cells *Energy Environ. Sci.* **8** 602

Bardeen J and Brattain W H 1948 The transistor, a semi-conductor triode *Phys. Rev.* **74** 230

De Simoni G, Paolucci F, Solinas P, Strambini E and Giazotto F 2018 Metallic supercurrent in field-effect transistor *Nat. Nanotechnol.* **13** 802

De Simoni G, Paolucci F, Puglia C and Giazotto F 2019 Josephson field-effect transistors based on all-metallic Al/Cu/Al proximity nanojunctions *ACS Nano* **13** 7871–6

Zaccone A and Trachenko K 2020 Explaining the low-frequency shear elasticity of confined liquids *Proc. Natl Acad. Sci.* **117** 19653

Ummarino G A and Zaccone A 2024 Quantitative Eliashberg theory of the superconductivity of thin films *J. Phys.: Condens. Matter* **37** 065703

Travaglino R and Zaccone A 2022 Analytical theory of enhanced Bose-Einstein condensation in thin films *J. Phys. B: At. Mol. Opt. Phys.* **55** 055301

Travaglino R and Zaccone A 2023 Extended analytical BCS theory of superconductivity in thin films *J. Appl. Phys.* **133** 033901

Phillips A E, Baggioli M, Sirk T W, Trachenko K and Zaccone A 2021 Universal $L-3$ finite-size effects in the viscoelasticity of amorphous systems *Phys. Rev. Mater.* **5** 035602

Yu Y, Yang C, Baggioli M, Phillips A E, Zaccone A, Zhang L, Kajimoto R, Nakamura M, Yu D and Hong L 2022 The $\omega 3$ scaling of the vibrational density of states in quasi-2d nanoconfined solids *Nat. Commun.* **13** 3649

Cioni M, Polino D, Rapetti D, Pesce L, Delle Piane M and Pavan G M 2023 Innate dynamics and identity crisis of a metal surface unveiled by machine learning of atomic environments *J. Chem. Phys.* **158** 124701

Valentinis D, van der Marel D and Berthod C 2016 Rise and fall of shape resonances in thin films of BCS superconductors *Phys. Rev.* B **94** 054516

Kittel C 2005 *Introduction to Solid State Physics* (Wiley)

Hill T L 1960 *An Introduction to Statistical Thermodynamics* (Addison-Wesley, Reading Massachusetts) pp 493–5

Zaccone A 2024 Quantum confinement theory of the heat capacity of thin films *Phys. Rev. Mater.* **8** 056001

Zink B L, Pietri R and Hellman F 2006 Thermal conductivity and specific heat of thin-film amorphous silicon *Phys. Rev. Lett.* **96** 055902

Yan S, Wang Y, Tao F and Ren J 2022 High-throughput estimation of phonon thermal conductivity from first-principles calculations of elasticity *J. Phys. Chem.* A **126** 8771

Larkin J M and McGaughey A J H 2014 Thermal conductivity accumulation in amorphous silica and amorphous silicon *Phys. Rev.* B **89** 144303

Braun J L, Baker C H, Giri A, Elahi M, Artyushkova K, Beechem T E, Norris P M, Leseman Z C, Gaskins J T and Hopkins P E 2016

Size effects on the thermal conductivity of amorphous silicon thin films *Phys. Rev.* B **93** 140201

Wang Y, Fan Z, Qian P, Caro M A and Ala-Nissila T 2023 Quantum-corrected thickness-dependent thermal conductivity in amorphous silicon predicted by machine learning molecular dynamics simulations *Phys. Rev.* B **107** 054303

Wang X and Huang B 2014 Computational study of in-plane phonon transport in si thin films *Sci. Rep.* **4** 6399

Balandin A A 2020 Phononics of graphene and related materials *ACS Nano* **14** 5170

Zhou X, Liu Y, Tang B, Wang J, Dong H, Xiu X, Chen S and Fan Z 2025 Million-atom heat transport simulations of polycrystalline graphene approaching first-principles accuracy enabled by neuroevolution potential on desktop gpus *J. Appl. Phys.* **137** 014305 [25] Antidormi A, Colombo L and Roche S 2020 Thermal transport in amorphous graphene with varying structural quality *2 D Materials* **8** 015028

Han Z and Ruan X 2023 Thermal conductivity of monolayer graphene: convergent and lower than diamond *Phys. Rev.* B **108** L121412

Bianconi A, Valletta A, Perali A and Saini N L 1998 Superconductivity of a striped phase at the atomic limit *Physica* C **296** 269

Valletta A, Bianconi A, Perali A and Saini N L 1997 Electronic and superconducting properties of a superlattice of quantum stripes at the atomic limit *Z. Phys.* B **104** 707

Rogers J, Cutler P, Feuchtwang T and Lucas A 1987 Quantum size effects in the Fermi energy and electronic density of states in a finite square well thin film model *Surf. Sci.* **181** 436

Batabyal R and Dev B 2014 Electronic structure in the crossover regimes in lower dimensional structures *Physica* E **64** 224 [31] Fuchs K 1938 The conductivity of thin metallic films according to the electron theory of metals *Math. Proc. Camb. Phil. Soc.* **34** 100–8

Sondheimer E 1952 The mean free path of electrons in metals *Adv. Phys.* **1** 1

Zhang C and Liu Y 2024 Electron-surface scattering from first-principles *ACS Nano* **18** 27433

Zaccone A 2025 Thickness-dependent conductivity of nanometric semiconductor thin films *Phys. Rev. Materials* **9** 046001 [35] MacHale J *et al* 2019 Exploring conductivity in ex-situ doped Si thin films as thickness approaches 5 nm *J. Appl. Phys.* **125** 225709 [36] Wan W, Yao Y, Sun L, Liu C-

C and Zhang F 2017 Topological, valleytronic and optical properties of monolayer pbs *Adv. Mater.* **29** 1604788

Stewart J C and Pyatt K D Jr 1966 Lowering of ionization potentials in plasmas *Astrophys. J.* **144** 1203

Bardeen J, Cooper L N and Schrieffer J R 1957 Theory of superconductivity *Phys. Rev.* **108** 1175

Cohen M L and Louie S G 2016 *Fundamentals of Condensed Matter Physics* (Cambridge University Press)

van Weerdenburg W M J, Kamlapure A, Fyhn E H, Huang X, van Mullekom N P E, Steinbrecher M, Krogstrup P, Linder J and Khajetoorians A A 2023 Extreme enhancement of superconductivity in epitaxial aluminum near the monolayer limit *Sci. Adv.* **9** eadf5500

Deshpande A, Pusskeiler J, Prange C, Rogge U, Dressel M and Scheffler M 2025 Tuning the superconducting dome in granular aluminum thin films *J. Appl. Phys.* **137** 013902

Bianconi A and Missori M 1994 High Tc superconductivity by quantum confinement *J. Phys. I* **4** 361

Blatt J M and Thompson C J 1963 Shape resonances in superconducting thin films *Phys. Rev. Lett.* **10** 332

Shanenko A A, Croitoru M D and Peeters F M 2007 Oscillations of the superconducting temperature induced by quantum well states in thin metallic films: numerical solution of the Bogoliubov–de Gennes equations *Phys. Rev.* B **75** 014519

Chiang T-C 2004 Superconductivity in thin films *Science* **306** 1900

Guo Y *et al* 2004 Superconductivity modulated by quantum size effects *Science* **306** 1915

Qin S, Kim J, Niu Q and Shih C-K 2009 Superconductivity at the two-dimensional limit *Science* **324** 1314

Marsiglio F and Carbotte J P 2008 Electron-phonon superconductivity *Superconductivity: Conventional and Unconventional*

Superconductors ed K H Bennemann and J B Ketterson (Springer) pp 73–162

Ummarino G 2013 Eliashberg theory *Emergent Phenomena in Correlated Matter*, ed E Pavarini, E Koch and U Schollwoeck

(Forschungszentrum Julich GmbH and Institute for Advanced Simulations) p 13.1–13.36

Dayan M 1978 Tunneling measurements on crystalline and granular aluminum *J. Low Temp. Phys.* **32** 643

Giri A, Tokina M, Prezhdo O and Hopkins P 2020 Electron-phonon coupling and related transport properties of metals and intermetallic alloys from first principles *Mater. Today Phys.* **12** 100175

Allen P B and Mitrovi´c B 1983 *Theory of Superconducting tc* (Academic) pp 1 − 92

López-Nu´nez˜ D, Montserrat Q P, Rius G, Bertoldo E, Torras-Coloma A, Martínez M and Forn-Díaz P 2023 Magnetic penetration depth of aluminum thin films (arXiv:2311.14119 [cond-mat.supr-con])

Ummarino G A and Zaccone A 2024 Can the noble metals (Au, Ag and Cu) be superconductors? *Phys. Rev. Mater.* **8** L101801

Ummarino G A and Zaccone A 2025 Possible superconductivity in very thin magnesium films *Condensed Matter* **10** 17

Leonardo A, Sklyadneva I Y, Silkin V M, Echenique P M and Chulkov E V 2007 *Abinitio* calculation of the phonon-induced contribution to the electron-state linewidth on the Mg(0001) surface versus bulk Mg *Phys. Rev.* B **76** 035404

Preobrajenski A, Vinogradov N, Duncan D A, Lee T-L, Tsitsvero M, Taketsugu T and Lyalin A 2024 Boron-induced transformation of ultrathin Au films into two-dimensional metallic nanostructures *Nat. Commun.* **15** 10518

Liu Z, Han G, Sohn S, Liu N and Schroers J 2019 Nanomolding of crystalline metals: the smaller the easier *Phys. Rev. Lett.* **122** 036101

Ruf L *et al* 2024 Gate control of superconducting current: mechanisms, parameters and technological potential *Appl. Phys. Rev.* **11** 041314

Mukhanov O, Gupta D, Kadin A and Semenov V 2004 Superconductor analog-to-digital converters *Proc. IEEE* **92** 1564 [61] Tolpygo S K 2016 Superconductor digital electronics: scalability and energy efficiency issues (Review Article) *Low Temp. Phys.* **42** 361

Gambetta J M, Chow J M and Steffen M 2017 Building logical qubits in a superconducting quantum computing system *npj Quantum Inf.* **3** 2

Piatti E, Romanin D, Gonnelli R S and Daghero D 2018 Anomalous screening of an electrostatic field at the surface of niobium nitride *Appl. Surf. Sci.* **461** 17

Piatti E, Daghero D, Ummarino G A, Laviano F, Nair J R, Cristiano R, Casaburi A, Portesi C, Sola A and Gonnelli R S 2017 Control of bulk superconductivity in a BCS superconductor by surface charge doping via electrochemical gating *Phys. Rev.* B **95** 140501

Tajmar M 2008 Electrodynamics in superconductors explained by proca equations *Phys. Lett.* A **372** 3289

Hirsch J E 2004 Electrodynamics of superconductors *Phys. Rev.* B **69** 214515

Zaccone A and Fomin V M 2024 Theory of superconductivity in thin films under an external electric field *Phys. Rev.* B **109** 144520

Cooper L N 1956 Bound electron pairs in a degenerate Fermi gas *Phys. Rev.* **104** 1189

Weisskopf V F 1981 The formation of Cooper pairs and the nature of superconducting currents *Contemp. Phys.* **22** 375

Landau L D and Lifshitz E M 1981 *Quantum Mechanics: Non-Relativistic Theory* (Butterworth-Heinemann)

Zaccone A, Ummarino G A, Braggio A and Giazotto F 2025 Microscopic mechanism of electric field-induced superconductivity suppression in metallic thin films (arXiv:2502.08459 [cond-mat.supr-con])

de Gennes P 1979 *Scaling Concepts in Polymer Physics* (Cornell University Press)

Sidorova M *et al* 2020 Electron energy relaxation in disordered superconducting NbN films *Phys. Rev.* B **102** 054501

Setty C, Baggioli M and Zaccone A 2024 Anharmonic theory of superconductivity and its applications to emerging quantum materials *J. Phys.: Condens. Matter* **36** 173002

Jiang C, Beneduce E, Baggioli M, Setty C and Zaccone A 2023 Possible enhancement of the superconducting T_c due to sharp Kohn-like soft phonon anomalies *J. Phys.: Condens. Matter* **35** 164003

Baggioli M, Setty C and Zaccone A 2020 Effective theory of superconductivity in strongly coupled amorphous materials *Phys. Rev.* B **101** 214502

Jiang C, Alberto Ummarino G, Baggioli M, Liarokapis E and Zaccone A 2024 Correlation between optical phonon softening and superconducting T_c in $YBa_2Cu_3O_x$ within d-wave Eliashberg theory *J. Phys. Mater.* **7** 045002

Shokri S *et al* 2024 Evolution of dissipative regimes in atomically thin bi2sr2cacu2o8 + superconductor *Adv. Electron. Mater.*

n/a 2400496

Zaccone A 2024 Explaining the thickness-dependent dielectric permittivity of thin films *Phys. Rev.* B **109** 115435

Yu P, Wu J, Liu S, Xiong J, Jagadish C and Wang Z M 2016 Design and fabrication of silicon nanowires towards efficient solar cells *Nano Today* **11** 704

Baraban L, Ibarlucea B, Baek E and Cuniberti G 2019 Hybrid silicon nanowire devices and their functional diversity *Adv. Sci.* **6** 1900522

Joyce H J, Boland J L, Davies C L, Baig S A and Johnston M B 2016 A review of the electrical properties of semiconductor nanowires: insights gained from terahertz conductivity spectroscopy *Semicond. Sci. Technol.* **31** 103003

Fomin V M 2014 *Physics of Quantum Rings* (Springer)

Landr`o E, Fomin V M and Zaccone A 2025 Topological Bardeen–Cooper–Schrieffer theory of superconducting quantum rings *Eur. Phys. J. B* **98** 7

Wang J *et al* 2023 Experimental observation of berry phases in optical möbius-strip microcavities *Nat. Photon.* **17** 120

Marino E, Kodger T E, Wegdam G H and Schall P 2018 Revealing driving forces in quantum dot supercrystal assembly *Adv. Mater.* **30** 1803433

Mirigliano M, Borghi F, Podest`a A, Antidormi A, Colombo L and Milani P 2019 Non-ohmic behavior and resistive switching of au cluster-assembled films beyond the percolation threshold *Nanoscale Adv.* **1** 3119

Valletta A, Bianconi A, Perali A, Logvenov G and Campi G 2024 High-T_c superconducting dome in artificial heterostructures made of nanoscale quantum building blocks *Phys. Rev.* B **110** 184510